Recent trends in X-ray based characterization of nodular cast iron

Andriollo, Tito; Xu, Chaoling; Zhang, Yubin; Tiedje, Niels Skat; Hattel, Jesper Henri

Published in:
Material Design and Processing Communications

Link to article, DOI:
10.1002/mdp2.212

Publication date:
2021

Document Version
Peer reviewed version

Andriollo Tito (Orcid ID: 0000-0002-1873-0031)

Title:

Recent trends in X-ray based characterization of nodular cast iron

Running title:

Trends in X-ray characterization of nodular iron

Authors and Affiliations:

Tito Andriollo*, Chaoling Xu, Yubin Zhang, Niels Skat Tiedje, Jesper Hattel

Department of Mechanical Engineering, Technical University of Denmark, Denmark

* Corresponding author. Full address: Produktionstorvet, Building 425, room 214, 2800 Kgs. Lyngby, Denmark. E-mail: titoan@mek.dtu.dk

Acknowledgements:

The work received support from the Danish Research Council for Independent Research, grant no. 8022-00085B.

Abstract

Through various examples, this short review presents the main X-ray based techniques that are available to characterize nodular cast iron at the microstructural level. Emphasis is placed on the enormous potential offered by the recent developments in X-ray tomography, X-ray diffraction and digital volume correlation, which allow collecting microstructural and micromechanical information in 4D (3D plus time) during both casting and subsequent mechanical loading. The goal is to demonstrate that for nodular cast iron, which has an inherently three-dimensional, composite microstructure, X-ray based techniques provide some significant advantages over conventional microscopy. For this reason, these techniques can be instrumental in unveiling the mechanisms controlling both the formation of the microstructure

as well as its micro-mechanical behavior during in-service loading, thus paving the way to the development of improved process-structure-property relations.

Keywords

Cast iron; X-rays; 4D characterization; Tomography; Diffraction; Digital Volume Correlation

1 Introduction

In nodular cast iron, also known as ductile iron (DI), minimal fluctuations of the process parameters can result in microstructural variations that severely alter the mechanical behavior of the material under in-service loading. This represents a serious obstacle to increasing the material reliability and expanding its application realm. Therefore, achieving improved understanding of the mechanisms controlling both the solidification and the subsequent mechanical response is imperative.

Traditional conceptual models for solidification of DI were developed based on experimentally measured cooling curves and analyses of 2D micrographs at room temperature [1–5]. Such conceptual models have been used to develop several mathematical models which provide quantitative descriptions of the main solidification stages. Yet, none of the theories that have been presented over the years can provide a unified picture of the graphite nucleation and growth over a wide range of process conditions [6,7]. One reason is that most of the models available today are based on strictly simplified geometrical assumptions. Typically it is assumed that graphite grows spherically, and that it is completely and uniformly encapsulated by austenite [7]. Off eutectic austenite can be modelled, but how the phases impinge on each other in three dimensions during the final part of solidification and how this impingement influences the shape and distribution of graphite has not been modelled successfully. As a consequence, the models can capture global trends, but fall short of providing satisfactory results in presence of localized and inherently 3D effects like e.g. graphite degeneration [8]. This creates the need for 3D techniques that can capture, visualize and ultimately explain via more sophisticated models the complex solidification process of DI.

A similar need exists with respect to the connection between the microstructure and the final mechanical properties of DI. Several ex-situ and in-situ investigations based on 2D microscopy have been carried out with the aim of clarifying the micro-mechanical interactions among the microstructural constituents during mechanical loading (see e.g. [9–11] and the references therein). However, the generalization of 2D surface observations to statements with general validity has always been critical. This is because the spherical shape of the graphite invariably

induces a triaxial stress state in the bulk of the microstructure, as opposed to the biaxial stress state existing at the surface [12,13]. Moreover, "hidden" graphite particles located just below the observation surface can have a strong impact on localized phenomena like plastic deformation and crack formation [14,15], which may go unnoticed unless full 3D examinations are conducted.

The following sections will show that the powerful X-ray-based techniques available today can be instrumental in this context, as they allow conducting 4D studies of key microstructural-level phenomena occurring during solidification, solid-state cooling and room-temperature mechanical loading. It must be emphasized that a thorough review is beyond the scope of the present manuscript. The focus here is rather on providing a list of examples that serve to highlight current capabilities and limitations of X-ray-based characterization of DI.

2 Solidification

During solidification of DI, spheroidal graphite particles (GPs) and pro-eutectic austenite nucleate independently in the liquid. After a short stage of growth, the GPs are partially/fully engulfed by austenite and their growth becomes governed by the diffusion of carbon from the remaining liquid through the austenite shell. The final solidified microstructure plays a crucial role in determining the mechanical properties of DI, and thus a comprehensive understanding of these two solidification stages is essential to optimize the material performance.

The use of intense synchrotron X-rays enables capturing the solidification process of DI. By 2D radiography performed using X-rays with relatively low energy [16], it is possible to distinguish austenite from liquid, and therefore clarify the solidification sequence. New and deeper understanding of the importance of Mg addition on the solidification sequence [17–19], the nucleation frequency of GPs [18] as well as the floating of primary GPs [20] have been obtained based on in-situ radiographic examinations. However, the 2D radiographic experiments have the natural limitation that the actual sizes and shapes of GPs cannot be determined. Additionally, the 2D geometric confinement has been confirmed to be incongruent with conditions under which the solidification of a 3D component takes place. The results obtained are thus not representative of bulk materials; 3D characterization is therefore highly demanded.

The first 4D (x, y, z, time) study of the solidification of DI was carried out at Diamond Light Source by means of X-ray tomography [8]. X-ray tomography is the acquisition of a sequence of projection images of a sample, which is rotated at constant speed at progressively increasing view angles [21]. By reconstructing the set of projection images taken from a 360° rotation,

the 3D microstructure of the sample is obtained. In the mentioned study [8], the dynamic nucleation and growth of the GPs was evaluated using a 70 keV monochromatic beam with a spatial resolution of 5 μm × 5 μm × 5 μm and a temporal resolution of 40 s (Figure 1). Such 4D characterization allowed not only to investigate mechanisms but also to study the nucleation and growth kinetics of hundreds of GPs with unprecedented level of detail. In particular, the nucleation rate of graphite was found to increase exponentially once a critical undercooling was reached, peaking and then declining sharply. Similarly, the GPs growth rate increased initially, peaked and then reduced in the later stage of solidification. Concerning the formation of degenerate graphite, which is often regarded as an element of concern for its negative impact on the mechanical properties [22,23], a striking result was obtained. In the beginning, GPs nucleated and grew with spheroidal shape and degenerate features emerged from them later on during solidification, e.g. the formation of 'polyp-like' extensions and the formation of spheroidal blobs at the free ends of the polyps.

Synchrotron tomography investigations of the solidification of DI were also performed using pink X-ray beam [20]. Compared to monochromatic beam, the use of X-rays with a broader spectrum can substantially improve the temporal resolution, by a factor of ~80-100, to 0.5 s, respectively. Owing to the relatively high temporal resolution, the floating of GPs was captured and shown to stop when the GPs were engulfed by austenite dendrites [20]. Furthermore, secondary nucleation between the primary GPs nucleated earlier and engulfed by austenite dendrites was directly observed. The high temporal resolution also allows evaluation of the floating distance of GPs. It was found that the floating distance of the secondary GPs is much shorter than that of primary GPs, suggesting that the secondary GPs nucleate in the austenite dendrite network and are engulfed immediately by the austenite dendrites. In addition, the number of secondary GPs is larger than that of primary GPs, which implies that engulfment of GPs into the austenite dendrites contributes to increasing the number of GPs during solidification by incrementing the driving force for their nucleation.

Overall, it can be concluded that the time-resolved 3D X-ray tomography studies conducted so far have captured the dynamic processes of the nucleation, growth and floating of GPs, and highlighted how the degenerate features develop from spheroidal GPs. These findings are crucial for the development of advanced models where some of the simplifying assumptions associated with the traditional solidification models are relaxed [24].

3 Solid-state cooling

During solid-state cooling, mechanical stress can build up locally around the GPs due to volumetric mismatch with the surrounding matrix [25]. At temperatures above the lower inter-critical temperature (~790 °C), the main cause of such volumetric mismatch is the significant growth of the GPs due to Carbon diffusion from the surrounding austenite. As the austenite is soft, the volumetric mismatch can be accommodated by matrix creep. By contrast, as the temperature drops below the lower inter-critical temperature, the strength of the matrix increases [26] and thermal stress due to the difference in thermal expansion between the GPs and the matrix can build up [25,27,28]. The magnitude and distribution of this thermal stress locally around individual GPs are important for the mechanical properties of DI [25,29], and have to be characterized in detail in order to optimize the processing route and mechanical properties of DI.

Over the past two decades, significant effort has been devoted to the development of synchrotron techniques for characterizing 3D grain structure and local stresses, including 3D X-ray Laue microdiffraction (3DμXRD) [30–32], and 3D X-ray diffraction (3DXRD) [33,34] and its variants: high-energy X-ray diffraction microscopy [35,36], diffraction contrast tomography [37,38] , dark field X-ray microscopy [39,40] and scanning 3DXRD [41]. Among these techniques, 3DμXRD is in particular suitable for mapping microstructure and strain/stress state in bulk samples, as it can provide a spatial resolution of submicrometer, angular resolution of 0.01° and a strain resolution of 1×10^{-4} [32,42].

Recently, 3DμXRD has been used to characterize microstructure and elastic strains around individual GPs fully embedded in ferrite matrix grains in two DI samples manufactured using different molds: either a metal or a sand mold [27,43]. These studies conducted at room temperature can shed light on the formation of local residual stresses at GPs. Examples of microstructure are shown in Figure 2. The GP size covered in these studies ranges from 30 to 150 μm. With the high angular resolution of the 3DμXRD operated using a polychromatic beam, the results reveal that the ferrite matrix in both samples is plastically deformed, containing dislocation boundaries with low misorientation angles. Beside the known fact that fast cooling rate leads on average to a smaller GP size and smaller ferrite grain size, the results further shows that fast cooling rate by the metal mold results in more dislocation boundaries with finer spacing than slow cooling rate with the sand mold.

The high angular resolution orientation data from the polychromatic 3DμXRD allows further a unique quantification of local plastic deformation. As shown in Figure 3, the results of local

dislocation density determined based on the local misorientations for regions at different distances from the GP/matrix interfaces reveal evidently a gradient in dislocation densities in the matrix. And the strain gradient is affected by the GP size and is very pronounced for the smallest GP. If the dislocation density is plotted as a function of the reciprocal GP size, $1/R_{GN}$, a reasonably good linear relationship is found for regions with the same normalized distances (see Figure 3b). Based on the mechanism-based theory of strain gradient plasticity [44], this result suggests that the plastic strain field averaged over all matrix grains around the GPs is about the same for different GPs when normalized by R_{GN}. That means the plastic strain field is scaling with the GP size, even though locally, different grains deformed differently.

A similar scaling behavior is also seen for the residual elastic strains locally around the GPs (see Figure 4), which are obtained using the 3DμXRD operated using a monochromatic beam [31]. On average, this is in good accord with the prediction by classic analytical models [45–48], and it reveals that the cooling rate has a minor effect on the residual elastic strain. Nevertheless, a large scatter in strain is seen for the regions close to the GP/matrix interface. A finite element study suggests that this result is likely to be related to the internal structure of the GPs [49].

The maximum residual stress values estimated based on directional Young's moduli and the elastic strains are in the range 110-180 MPa. This range can be compared to the yield stress of the ferrite matrix, which is about 300 MPa at room temperature [25], and should be taken into account in developing advanced models with high predictabilities and understanding the plastic deformation the DI [29].

Since the measurements are non-destructive, 3DμXRD provides further possibilities to follow the evolution of both microstructure and strains/stresses in 3D during in-/ex-situ annealing or plastic deformation [50–52]. Such 4D data sets would be very valuable for tailoring both microstructure and micro-strain for optimizing the materials mechanical properties of DI.

4 Mechanical loading

The limitations of 2D methods mentioned in the introduction have fostered the application of 3D techniques to study the microstructural behavior of DI under mechanical loading. X-ray Computed Tomography (CT) in particular is well suited to this purpose, owing to the good contrast between the graphite and the surrounding matrix. As early as almost two decades ago, X-ray CT was used to investigate the complex 3D shape of short cracks nucleated during cyclic loading [53,54], thus demonstrating the relevance of the technique within the context of fatigue investigations. Later, in-situ experiments were also conducted with the purpose of tracking the

growth of fatigue cracks over time [55]. In addition to the detection of cracks, X-ray CT has proved to be an excellent tool for the fast and accurate reconstruction of the graphite morphology [56], which is known to be strongly linked to the material mechanical properties [57]. In this context, X-ray CT represents a fast alternative to serial sectioning combined with optical microscopy and it is particularly useful in presence of irregular particles, since a statistical analysis of the graphite shape based on 2D images is not accurate in such a case [58]. Compared to optical microscopy, a limitation of X-ray CT is the difficulty of separating the small GPs from the porosities, due to the lack of sufficient contrast [59]. However, it is foreseen that image analysis techniques, possibly supported by machine learning, might solve this issue in the future. In fact, contrast-enhancing techniques based on image analysis have already been applied to distinguish the pearlite from the ferrite in DI with ferritic-pearlitic matrix [60].

The potential of X-ray CT has been enhanced greatly by the advent of Digital Volume Correlation (DVC). As described in detail elsewhere, e.g. [61], DVC allows constructing a mapping in the form of a displacement function between two CT scans: one taken before and one taken after (or during) mechanical loading. The displacement function is determined by tracking the movement of a characteristic pattern that, for DI, corresponds to the GP distribution. The displacement can be used to derive the strain, meaning that the combination of X-ray CT and DVC provides access to local micro-mechanical information relating to the type of loading/deformation the material is subjected to (see Figure 5). This fact was exploited in a pioneering work to determine the evolution of the stress intensity factor during propagation of a fatigue crack in DI from in-situ measurements of the strain field near the crack front [62,63]. The technique was subsequently used to investigate several localized effects that could not be captured with 2D methods. Among these are the impact of the crack front curvature [64] and the role played by the 3D shape and orientation of the GPs [65] during fatigue crack propagation. With respect to monotonic loading, the effect of the graphite spatial arrangement on the ductile damage mechanisms in presence of complex stress states was deeply investigated, and correlations between the evolution of the volumetric part of the local strain and the dominant failure mechanisms were unraveled [66]. The possibility to couple X-ray CT and DVC with post-mortem metallographic examinations was explored as well, and used to reveal the connection between the plastic shear bands forming during tensile loading and the complex morphology of the first-to-solidify regions [67].

An important aspect of DVC is that it enables a synergistic integration not only with X-ray CT, but also with numerical models. A first reason is that the model domain can be limited to a

small region of interest that does not need to include the points where the external loads are applied. This is because the displacement data from DVC – instead of the external loads – can be used to prescribe the boundary conditions in the model [68,69]. A second reason is that the displacement and strain fields reconstructed with DVC can be used to validate the models at the level of the microstructure, which is highly valuable since the X-ray CT data allows setting up models where the real microstructure can be fully resolved [70]. These two facts mean that it is nowadays possible to setup numerical models with superior accuracy and predictive power compared to the idealized unit cell models that have traditionally been used to study the micro-mechanics of DI in the past [29]. That is, by exploiting models that integrate information from X-ray CT and DVC the interaction between the microstructural constituents upon mechanical loading can be quantified and explained with unprecedented level of detail. An example of this is given in Figure 6, where the 3D reconstruction of a fatigue crack that grows by linking the GPs is depicted. The reconstruction, obtained by segmenting the DVC data, was used to setup a finite element model that unveiled a correlation between the local crack growth direction – which controls the crack roughness and thus affects the amount of energy dissipated – and the predicted micro-mechanical fields developing in between the GPs [71].

5 Conclusions and outlook

As demonstrated by the few example studies presented in this paper, state-of-the-art X-ray based techniques allow collecting 4D microstructural and micromechanical information in-situ during solidification, solid-state cooling and mechanical loading of DI. Due to the inherently three-dimensional, composite microstructure of this material, the collected data can provide insights that are hard or impossible to obtain with 2D or destructive 3D methods. Furthermore, the data enables the development and validation of numerical models that can describe the microstructural behavior of DI with greater fidelity level.

Even though the experimental tools at hand are very powerful, there is also a need for technique advancements. To distinguish the austenite from the liquid during solidification and thus reveal the interaction between the austenite and the GPs with greater accuracy, supplemental contrast modes such as diffraction and phase contrast could be adopted in the future. Addition of a segregating element to enhance the absorption contrast between the liquid phase and the solidified austenite could be considered also.

With the third generation synchrotron source, the scanning time for a reasonable sized 3D orientation and strain mapping with 3DμXRD is still quite long [51,52]. Upon further deformation, the situation becomes even worse [72]. Additionally, full stress tensor is required

in order to obtain a complete picture of the effects of local residual stresses on the mechanical properties. This requires strain mapping of at least three components along widely deviated directions, and is currently possible [73], but still need more technical development to ensure the accuracy of the obtained stress tensor results.

Concerning DVC-based investigations, a major limitation is the spatial resolution of the technique. Since the GPs are used as tracking markers, the former is limited to roughly the particle spacing. Consequently, it is not possible to capture information at a scale smaller than this limit. In this respect, a promising alternative is the application of 3DXRD and 3DμXRD, which, as already mentioned, provide information at the level of the individual matrix grains. A preliminary study suggests that 3DXRD is indeed applicable to DI and can be used to investigate the evolution of the grain-level strain during tensile loading [74].

At the time of writing, the fourth-generation synchrotron source is already available at MAXIV in Lund, Sweden and European Synchrotron Radiation Facility, in Grenoble, France. Advanced photon source in US has already planned to upgrade to the fourth-generation in the next couple of years [75], with aim to increase the undulator source brightness by a factor of ~100. Which such a brighter beam, the temporal resolution for the tomography and diffraction can be improved by a factor of 10-100, implying that time-resolved and full stress tensor measurements will be prevalent in the near future.

References

[1] C.R.J. Loper, Processing and control of ductile iron, AFS Trans. 77 (1969) 1–7.

[2] R.W. Heine, A model for specific volume and expansion and contraction behaviour of solidifying and cooling ductile and gray iron, AFS Trans. 96 (1988) 413–422.

[3] T. Skaland, O. Grong, T. Grong, A model for the graphite formation in ductile cast iron. I. inoculation mechanisms, Metall. Trans. A. 24A (1993) 2321–2345.

[4] K.M.K.M. Pedersen, N. Tiedje, Nucleation and solidification of thin walled ductile iron - Experiments and numerical simulation, Mater. Sci. Eng. A. 413–414 (2006) 358–362. doi:10.1016/j.msea.2005.08.158.

[5] G. Rivera, R. Boeri, J. Sikora, Revealing and characterising solidification structure of ductile cast iron, Mater. Sci. Technol. 18 (2002) 691–697. doi:10.1179/026708302225003668.

[6] M.I. Onsoien, O. Grong, O. Gundersen, T. Skaland, A process model for the microstructure evolution in ductile cast iron: Part I. the model, Metall. Mater. Trans. A-Physical Metall. Mater. Sci. 30 (1999) 1053–1068.

[7] G. Lesoult, M. Castro, J. Lacaze, Solidification of spheroidal graphite cast irons - I. Physical modelling, Acta Mater. 46 (1998) 983–995. doi:10.1016/S1359-6454(97)00281-4.

[8] M.A. Azeem, M.K. Bjerre, R.C. Atwood, N. Tiedje, P.D. Lee, Synchrotron quantification of graphite nodule evolution during the solidification of cast iron, Acta Mater. 155 (2018) 393–401. doi:10.1016/j.actamat.2018.06.007.

[9] C. Bellini, V. Di Cocco, G. Favaro, F. Iacoviello, L. Sorrentino, Ductile cast irons: Microstructure influence on the fatigue initiation mechanisms, Fatigue Fract. Eng. Mater. Struct. 42 (2019) 1–11. doi:10.1111/ffe.13100.

[10] F. Iacoviello, V. Di Cocco, C. Bellini, Fatigue crack propagation and damaging micromechanisms in Ductile Cast Irons, Int. J. Fatigue. (2019). doi:10.1016/j.ijfatigue.2019.02.030.

[11] K.A. Kasvayee, E. Ghassemali, K. Salomonsson, S. Sujakhu, S. Castagne, A.E.W. Jarfors, Microstructural strain mapping during in-situ cyclic testing of ductile iron, Mater. Charact. 140 (2018) 333–339. doi:10.1016/j.matchar.2018.04.017.

[12] J.H. Liu, X.Y. Hao, G.L. Li, G.S. Liu, Microvoid evaluation of ferrite ductile iron under strain, Mater. Lett. 56 (2002) 748–755.

[13] T. Andriollo, J. Thorborg, J. Hattel, The influence of the graphite mechanical properties on the constitutive response of a ferritic ductile cast iron - A micromechanical fe analysis, in: Proc. 8th Int. Conf. Comput. Plast. - Fundam. Appl. COMPLAS 2015, 2015: pp. 632–641.

[14] K.A. Kasvayee, K. Salomonsson, E. Ghassemali, A.E.W. Jarfors, Microstructural strain distribution in ductile iron; comparison between finite element simulation and digital image correlation measurements, Mater. Sci. Eng. A. 655 (2016) 27–35. doi:10.1016/j.msea.2015.12.056.

[15] D.O. Fernandino, V. Di Cocco, R. Boeri, F. Iacoviello, Microstrain measurements and damage analysis during tensile loading of intercritical austempered ductile iron, Fatigue Fract. Eng. Mater. Struct. (2020) 1–13. doi:10.1111/ffe.13346.

[16] P. Staron, A. Schreyer, H. Clemens, S. Mayer, Neutrons and Synchrotron Radiation in Engineering Materials Science: From Fundamentals to Applications, 2nd editio, 2008. doi:10.1002/9783527621927.

[17] K. Yamane, A. Sugiyama, T. Nagira, M. Yoshiya, H. Yasuda, Y. Tanaka, A. Satou, K. Uesugi, A. Takeuchi, Y. Suzuki, H. Honda, K. Satou, Influence of Mg Content on

Graphite Growth in Hypereutectic Cast Iron and Crystallographic Feature of Graphite, J. Japan Foundry Eng. Soc. 86 (2014) 461–470. doi:10.11279/jfes.86.461.

[18] K. Yamane, H. Yasuda, A. Sugiyama, T. Nagira, M. Yoshiya, K. Morishita, K. Uesugi, A. Takeuchi, Y. Suzuki, Influence of Mg on Solidification of Hypereutectic Cast Iron: X-ray Radiography Study, Metall. Mater. Trans. A Phys. Metall. Mater. Sci. 46 (2015) 4937–4946. doi:10.1007/s11661-015-3077-z.

[19] H. Yasuda, A. Sugiyama, T. Nagira, K. Morishita, M. Yoshiya, T. Nishimura, K. Yamane, Solidification sequence of ductile cast iron-In-situ observation and modeling, in: Proc. 72nd World Foundary Congr., 2016: pp. 257–258.

[20] K. Chatcharit, A. Sugiyama, K. Morishita, T. Narumi, K. Kajiwara, H. Yasuda, Time Evolution of Solidification Structure in Ductile Cast Iron with Hypereutectic Compositions, Int. J. Met. 14 (2020) 794–801. doi:10.1007/s40962-020-00424-3.

[21] A.J. Shahani, X. Xiao, E.M. Lauridsen, P.W. Voorhees, Characterization of metals in four dimensions, Mater. Res. Lett. 8 (2020) 462–476. doi:10.1080/21663831.2020.1809544.

[22] E. Foglio, D. Lusuardi, A. Pola, G.M. La Vecchia, M. Gelfi, Fatigue design of heavy section ductile irons: Influence of chunky graphite, Mater. Des. 111 (2016) 353–361. doi:10.1016/j.matdes.2016.09.002.

[23] R. Rizzoni, P. Livieri, R. Tovo, M. Cova, Development of a hierarchical model for voids clusters suitable for cast iron degenerated graphite, Theor. Appl. Fract. Mech. (2020) 102731. doi:10.1016/j.tafmec.2020.102731.

[24] M.K. Bjerre, M.A. Azeem, N.S. Tiedje, J. Thorborg, P.D. Lee, J.H. Hattel, A graphite nodule growth model validated by in situ synchrotron x-ray tomography, Model. Simul. Mater. Sci. Eng. 26 (2018). doi:10.1088/1361-651X/aae9ce.

[25] N. Bonora, A. Ruggiero, Micromechanical modeling of ductile cast iron incorporating damage. Part I: Ferritic ductile cast iron, Int. J. Solids Struct. 42 (2005) 1401–1424. doi:10.1016/j.ijsolstr.2004.07.025.

[26] R. Kaibyshev, I. Kazakulov, Deformation Behavior of Fe-3%Si Steel at High Temperatures, Key Eng. Mater. 171–174 (2000) 213–218. doi:10.4028/www.scientific.net/KEM.171-174.213.

[27] Y.B. Zhang, T. Andriollo, S. Fæster, W. Liu, J. Hattel, R.I. Barabash, Three-dimensional local residual stress and orientation gradients near graphite nodules in ductile cast iron, Acta Mater. 121 (2016) 173–180. doi:10.1016/j.actamat.2016.09.009.

[28] T. Andriollo, J. Thorborg, N. Tiedje, J. Hattel, A micro-mechanical analysis of thermo-elastic properties and local residual stresses in ductile iron based on a new anisotropic model for the graphite nodules, Model. Simul. Mater. Sci. Eng. 24 (2016). doi:10.1088/0965-0393/24/5/055012.

[29] T. Andriollo, Y.B. Zhang, S. Fæster, J. Thorborg, J. Hattel, Impact of micro-scale residual stress on in-situ tensile testing of ductile cast iron: Digital volume correlation vs. model with fully resolved microstructure vs. periodic unit cell, J. Mech. Phys. Solids. 125 (2019) 714–735. doi:10.1016/J.JMPS.2019.01.021.

[30] W. Yang, G.E. Ice, J.D. Budai, J.Z. Tischler, B.C. Larson, Three-dimensional X-ray structural microscopy with submicrometre resolution, Nature. 415 (2002) 887–890.

[31] L.E. Levine, B.C. Larson, W. Yang, M.E. Kassner, J.Z. Tischler, M.A. Delos-Reyes, R.J. Fields, W. Liu, X-ray microbeam measurements of individual dislocation cell elastic strains in deformed single-crystal copper., Nat. Mater. 5 (2006) 619–622. doi:10.1038/nmat1698.

[32] B.C. Larson, L.E. Levine, Submicrometre-resolution polychromatic three-dimensional X-ray microscopy, J. Appl. Crystallogr. 46 (2013) 153–164. doi:10.1107/S0021889812043737.

[33] H.F. Poulsen, Three-dimensional X-ray diffraction microscopy : mapping polycrystals and their dynamics, 2004.

[34] H.F. Poulsen, An introduction to three-dimensional X-ray diffraction microscopy, J. Appl. Crystallogr. 45 (2012) 1084–1097. doi:10.1107/S0021889812039143.

[35] R.M. Suter, D. Hennessy, C. Xiao, U. Lienert, Forward modeling method for microstructure reconstruction using x-ray diffraction microscopy: Single-crystal verification, Rev. Sci. Instrum. 77 (2006) 1–12. doi:10.1063/1.2400017.

[36] S.F. Li, R.M. Suter, Adaptive reconstruction method for three-dimensional orientation imaging, J. Appl. Crystallogr. 46 (2013) 512–524. doi:10.1107/S0021889813005268.

[37] W. Ludwig, S. Schmidt, E.M. Lauridsen, H.F. Poulsen, X-ray diffraction contrast tomography: a novel technique for three-dimensional grain mapping of polycrystals. I. Direct beam case, J. Appl. Crystallogr. 41 (2008) 302–309. doi:10.1107/S0021889808001684.

[38] P. Reischig, A. King, L. Nervo, N. Viganó, Y. Guilhem, W.J. Palenstijn, K.J. Batenburg, M. Preuss, W. Ludwig, Advances in X-ray diffraction contrast tomography: flexibility in the setup geometry and application to multiphase materials, J. Appl. Crystallogr. 46

(2013) 297–311. doi:10.1107/S0021889813002604.

[39] H. Simons, A.B. Haugen, A.C. Jakobsen, S. Schmidt, F. Stöhr, M. Majkut, C. Detlefs, J.E. Daniels, D. Damjanovic, H.F. Poulsen, Long-range symmetry breaking in embedded ferroelectrics, Nat. Mater. 17 (2018) 814–819. doi:10.1038/s41563-018-0116-3.

[40] S.R. Ahl, H. Simons, Y.B. Zhang, C. Detlefs, F. Stöhr, A.C. Jakobsen, D. Juul Jensen, H.F. Poulsen, Ultra-low-angle boundary networks within recrystallizing grains, Scr. Mater. 139 (2017) 87–91. doi:10.1016/j.scriptamat.2017.06.016.

[41] Y. Hayashi, Y. Hirose, Y. Seno, Polycrystal orientation mapping using scanning three-dimensional X-ray diffraction microscopy, J. Appl. Crystallogr. 48 (2015). doi:10.1107/S1600576715009899.

[42] Y. Zhang, R.I. Barabash, High Resolution Mapping of Orientation and Strain Gradients in Metals by Synchrotron 3D X-ray Laue Microdiffraction, (2019) 1–14. doi:10.3390/qubs3010006.

[43] Y.B. Zhang, T. Andriollo, S. Fæster, R. Barabash, R. Xu, N. Tiedje, J. Thorborg, J. Hattel, D. Juul Jensen, N. Hansen, Microstructure and residual elastic strain at graphite nodules in ductile cast iron analyzed by synchrotron X-ray microdiffraction, Acta Mater. 167 (2019) 221–230. doi:10.1016/j.actamat.2019.01.038.

[44] H. Gao, Y. Hang, W.D. Nix, J.W. Hutchinson, Mechanism-based strain gradient plasticity - I. Theory, J. Mech. Phys. Solids. 47 (1999) 1239–1263. doi:10.1016/S0022-5096(98)00103-3.

[45] H. Ledbetter, M. Austin, Internal strain (stress) in an SiC-Al particle-reinforced composite: an X-ray diffraction study, Mater. Sci. Eng. 89 (1987) 53–61.

[46] J.D. Eshelby, The determination of the elastic field of an ellipsoidal inclusion, and related problems, Proc. R. Soc. London A Math. Phys. Eng. Sci. 241 (1957) 376–396. doi:10.1098/rspa.1957.0133.

[47] E.U. Lee, Thermal stress and strain in a metal matrix composite with a spherical reinforcement particle, Metall. Trans. A. 23A (1992) 2205–2210.

[48] Y. Huang, H. Gao, W.D. Nix, J.W. Hutchinson, Mechanism-based strain gradient plasticity - II. Analysis, J. Mech. Phys. Solids. 48 (2000) 99–128. doi:10.1016/S0022-5096(99)00022-8.

[49] T. Andriollo, K. Hellström, M.R. Sonne, J. Thorborg, N. Tiedje, J. Hattel, Uncovering the local inelastic interactions during manufacture of ductile cast iron: How the

substructure of the graphite particles can induce residual stress concentrations in the matrix, J. Mech. Phys. Solids. 111 (2018) 333–357. doi:10.1016/j.jmps.2017.11.005.

[50] C.L. Zhang, Y.B. Zhang, G.L. Wul, W. Liu, D. Juul Jensen, A. Godfrey, Quantification of deformation microstructure at ultra-low tensile strain in pure Al prepared by spark plasma sintering, IOP Conf. Ser. Mater. Sci. Eng. 219 (2017) 3–9. doi:10.1088/1757-899X/219/1/012050.

[51] Y.B. Zhang, J.D. Budai, J.Z. Tischler, W. Liu, R. Xu, E.R. Homer, A. Godfrey, D. Juul Jensen, Boundary migration in a 3D deformed microstructure inside an opaque sample, Sci. Rep. 7 (2017) 4423. doi:10.1038/s41598-017-04087-9.

[52] C. Xu, Y. Zhang, A. Godfrey, G. Wu, W. Liu, J.Z. Tischler, Q. Liu, D. Juul Jensen, Direct observation of nucleation in the bulk of an opaque sample, Sci. Rep. 7 (2017) 42508. doi:10.1038/srep42508.

[53] T.J. Marrow, H. Çetinel, S. Macdonald, P.J. Withers, A. Venslovas, M. Leonavičius, X-ray Tomography of Short Fatigue Cracks in Ductile Iron, in: 14th Eur. Conf. Fract., 2002.

[54] T.J. Marrow, H. Çetinel, M. Al-Zalmah, S. Macdonald, P.J. Withers, J. Walton, Fatigue crack nuclei in austempered ductile cast iron, Fatigue Fract. Eng. Mater. Struct. 25 (2002) 635–648. doi:10.1046/j.1460-2695.2002.00503.x.

[55] C. Verdu, J. Adrien, J.Y. Buffière, Three-dimensional shape of the early stages of fatigue cracks nucleated in nodular cast iron, Mater. Sci. Eng. A. 483–484 (2008) 402–405. doi:10.1016/j.msea.2006.09.178.

[56] A. Velichko, C. Holzapfel, F. Mücklich, 3D Characterization of Graphite Morphologies in Cast Iron, Adv. Eng. Mater. 9 (2007) 39–45. doi:10.1002/adem.200600175.

[57] D.M. Stefanescu, Mechanical Properties of Ductile Irons, in: D.M. Stefanescu (Ed.), ASM Handbook, Vol. 1A, Cast Iron Sci. Technol., ASM International, 2017: p. 600.

[58] S.N. Lekakh, X. Zhang, W. Tucker, H.K. Lee, T. Selly, J.D. Schiffbauer, Micro-CT quantitative evaluation of graphite nodules in SGI, Int. J. Met. 14 (2020) 318–327. doi:10.1007/s40962-019-00354-9.

[59] K. Mukherjee, S. Fæster, N. Hansen, A.B. Dahl, C. Gundlach, J.O. Frandsen, A. Sturlason, Graphite nodules in fatigue-tested cast iron characterized in 2D and 3D, Mater. Charact. 129 (2017) 169–178. doi:10.1016/j.matchar.2017.04.024.

[60] K. Salomonsson, J. Olofsson, Analysis of Localized Plastic Strain in Heterogeneous Cast Iron Microstructures Using 3D Finite Element Simulations, in: P. Mason, C.R.

Fisher, R. Glamm, M. V Manuel, G.J. Schmitz, A.K. Singh, A. Strachan (Eds.), Proc. 4th World Congr. Integr. Comput. Mater. Eng. (ICME 2017), Springer International Publishing, Cham, 2017: pp. 217–225. doi:10.1007/978-3-319-57864-4_20.

[61] A. Buljac, C. Jailin, A. Mendoza, J. Neggers, T. Taillandier-Thomas, A. Bouterf, B. Smaniotto, F. Hild, S. Roux, Digital Volume Correlation: Review of Progress and Challenges, Exp. Mech. 58 (2018) 661–708. doi:10.1007/s11340-018-0390-7.

[62] N. Limodin, J. Réthoré, J.Y. Buffière, A. Gravouil, F. Hild, S. Roux, Crack closure and stress intensity factor measurements in nodular graphite cast iron using three-dimensional correlation of laboratory X-ray microtomography images, Acta Mater. 57 (2009) 4090–4101. doi:10.1016/j.actamat.2009.05.005.

[63] N. Limodin, J. Réthoré, J.Y. Buffière, F. Hild, S. Roux, W. Ludwig, J. Rannou, A. Gravouil, Influence of closure on the 3D propagation of fatigue cracks in a nodular cast iron investigated by X-ray tomography and 3D volume correlation, Acta Mater. 58 (2010) 2957–2967. doi:10.1016/j.actamat.2010.01.024.

[64] J. Lachambre, J. Réthoré, A. Weck, J.Y. Buffiere, Extraction of stress intensity factors for 3D small fatigue cracks using digital volume correlation and X-ray tomography, Int. J. Fatigue. 71 (2015) 3–10. doi:10.1016/j.ijfatigue.2014.03.022.

[65] J. Hosdez, N. Limodin, D. Najjar, J.-F. Witz, E. Charkaluk, P. Osmond, A. Forré, F. Szmytka, Fatigue crack growth in compacted and spheroidal graphite cast irons, Int. J. Fatigue. (2019) 105319. doi:https://doi.org/10.1016/j.ijfatigue.2019.105319.

[66] A. Buljac, L. Helfen, F. Hild, T.F. Morgeneyer, Effect of void arrangement on ductile damage mechanisms in nodular graphite cast iron: In situ 3D measurements, Eng. Fract. Mech. 192 (2018) 242–261. doi:10.1016/j.engfracmech.2018.01.008.

[67] C.L. Xu, T. Andriollo, Y.B. Zhang, J.C. Hernando, J. Hattel, N. Tiedje, Micromechanical impact of solidification regions in ductile iron revealed via a 3D strain partitioning analysis method, Scr. Mater. 178 (2020) 463–467. doi:10.1016/j.scriptamat.2019.12.018.

[68] A. Buljac, M. Shakoor, J. Neggers, M. Bernacki, P.O. Bouchard, L. Helfen, T.F. Morgeneyer, F. Hild, Numerical validation framework for micromechanical simulations based on synchrotron 3D imaging, Comput. Mech. 59 (2017) 419–441. doi:10.1007/s00466-016-1357-0.

[69] M. Shakoor, A. Buljac, J. Neggers, F. Hild, T.F. Morgeneyer, L. Helfen, M. Bernacki, P.-O. Bouchard, On the choice of boundary conditions for micromechanical simulations

based on 3D imaging, Int. J. Solids Struct. 112 (2017) 83–96. doi:https://doi.org/10.1016/j.ijsolstr.2017.02.018.

[70] A. Buljac, V.M. Trejo Navas, M. Shakoor, A. Bouterf, J. Neggers, M. Bernacki, P.O. Bouchard, T.F. Morgeneyer, F. Hild, On the calibration of elastoplastic parameters at the microscale via X-ray microtomography and digital volume correlation for the simulation of ductile damage, Eur. J. Mech. A/Solids. 72 (2018) 287–297. doi:10.1016/j.euromechsol.2018.04.010.

[71] T. Andriollo, Y. Zhang, S. Fæster, V. Kouznetsova, Analysis of the correlation between micro-mechanical fields and fatigue crack propagation path in nodular cast iron, Acta Mater. 188 (2020) 302–314. doi:https://doi.org/10.1016/j.actamat.2020.02.026.

[72] S. Dhar, Y. Zhang, R. Xu, H.K. Danielsen, D. Juul Jensen, Synchrotron X-ray measurement of residual strain within the nose of a worn manganese steel railway crossing, in: IOP Conf. Ser. Mater. Sci. Eng., 2017. doi:10.1088/1757-899X/219/1/012016.

[73] L.E. Levine, C. Okoro, R. Xu, Full elastic strain and stress tensor measurements from individual dislocation cells in copper through-Si vias, IUCrJ. 2 (2015) 635–642. doi:10.1107/S2052252515015031.

[74] T. Sjögren, S. Hall, L. Elmquist, E. Dartfeldt, E. Larsson, M. Majkut, J. Elfsberg, P. Skoglund, J. Engqvist, In situ analysis of cast irons mechanical behaviour using synchrotron x-ray tomography and 3DXRD, IOP Conf. Ser. Mater. Sci. Eng. 861 (2020) 12039. doi:10.1088/1757-899x/861/1/012039.

[75] R. Haeffner, APS-U Beamline Update, St. Paul, MN, USA, 2017.

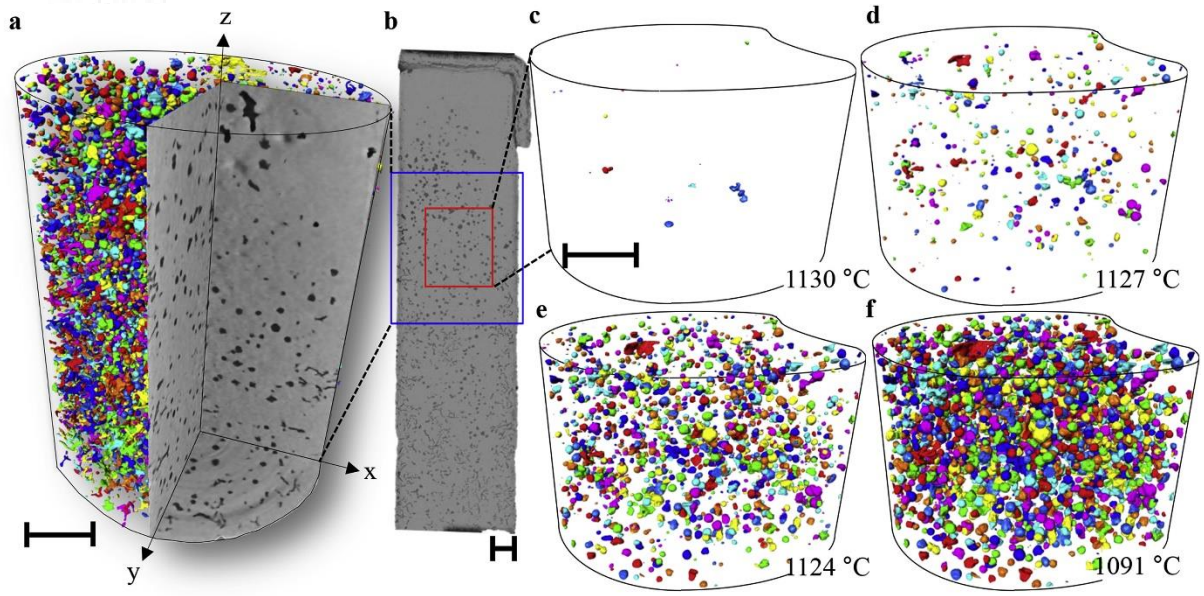

Figure 1. Tomography images revealing (a) multitude of graphite morphologies observed in 3D after solidification, (b) the post-solidification graphite morphologies in the entire 8mm sample at room temperature. The evolution of graphite nodules in the central volume is shown in 3D in (c)-(f), corresponding to a temperature range of 33 °C. Scale bar = 300 µm. Reproduced from [8].

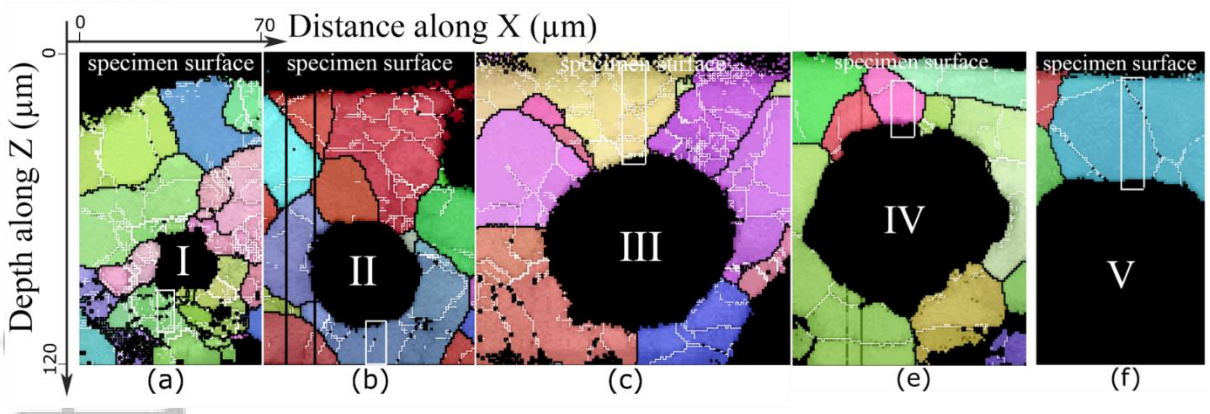

Figure 2. Microstructures of DI characterized using 3DμXRD. (a) - (e) showing microstructures around the selected GPs, I - V, respectively. GPs I-III and IV-V are from DI samples prepared using metal mold and sand mold, respectively. The cooling rate in the temperature range 810-500 °C is estimated qualitatively to be ~20 times faster for the sample prepared by the metal mold than that by the sand mold. In the maps, dislocation boundaries with misorientation angles in the range of 0.1 – 1°, 1 – 3°, and > 3° are shown in thin white, thick white and thick black lines, respectively. The colors of the matrix grains correspond to the crystallographic orientation along the specimen normal direction. The black pixels in the matrix away from the GPs are non-indexed. The five white boxes mark regions where elastic strains were measured. Reproduced from [43].

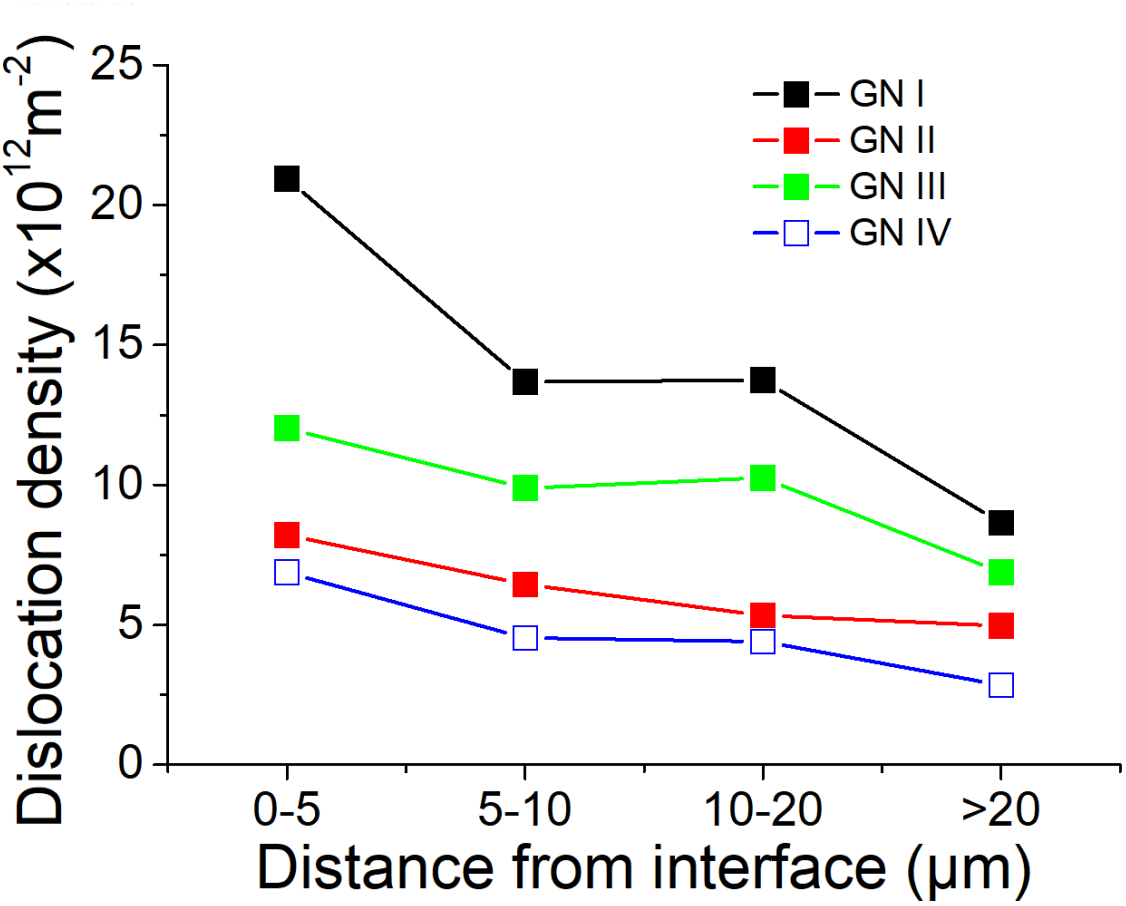

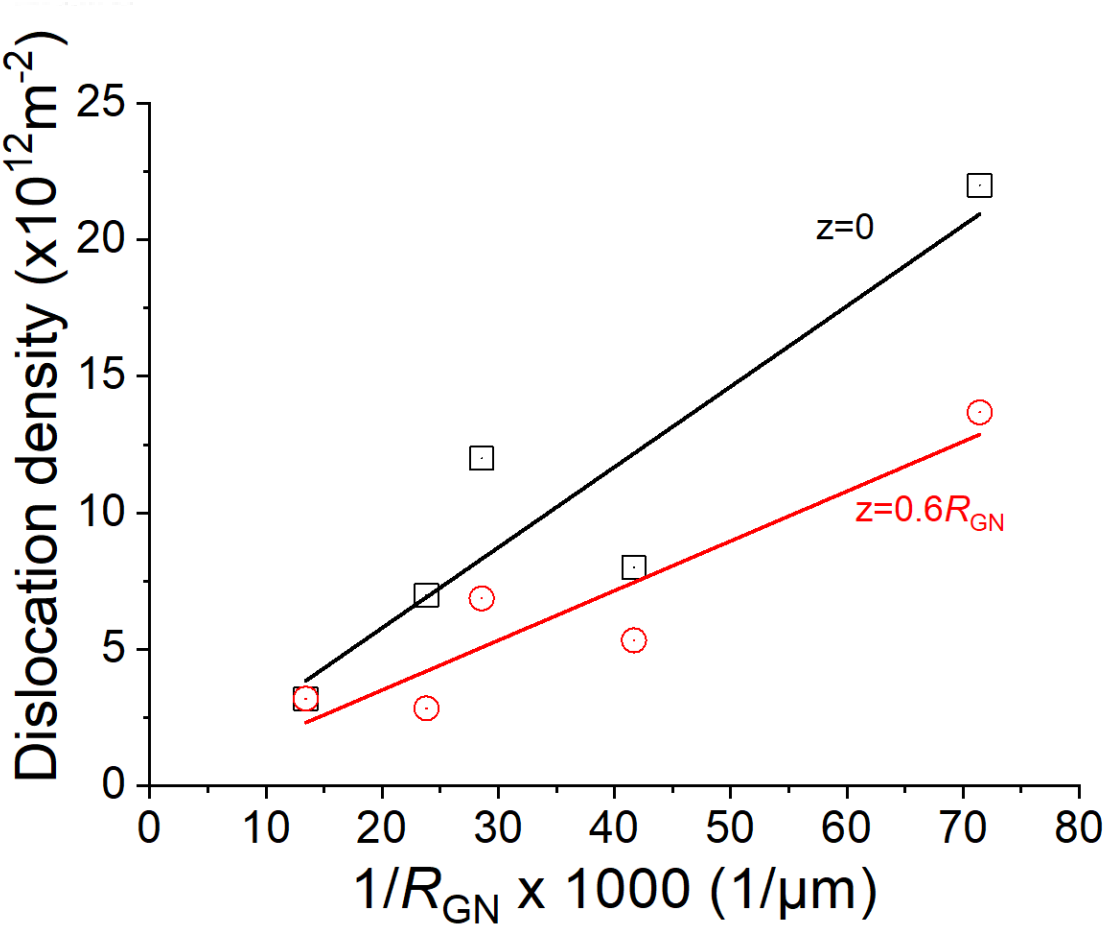

Figure 3. (a) Local average dislocation density as a function of distance from the GP/matrix interface. (b) Relationship between average local GP grain size, R_{GP}, and local dislocation density at $z \approx 0$ and $z \approx 0.6R_{GP}$. Reproduced from [43].

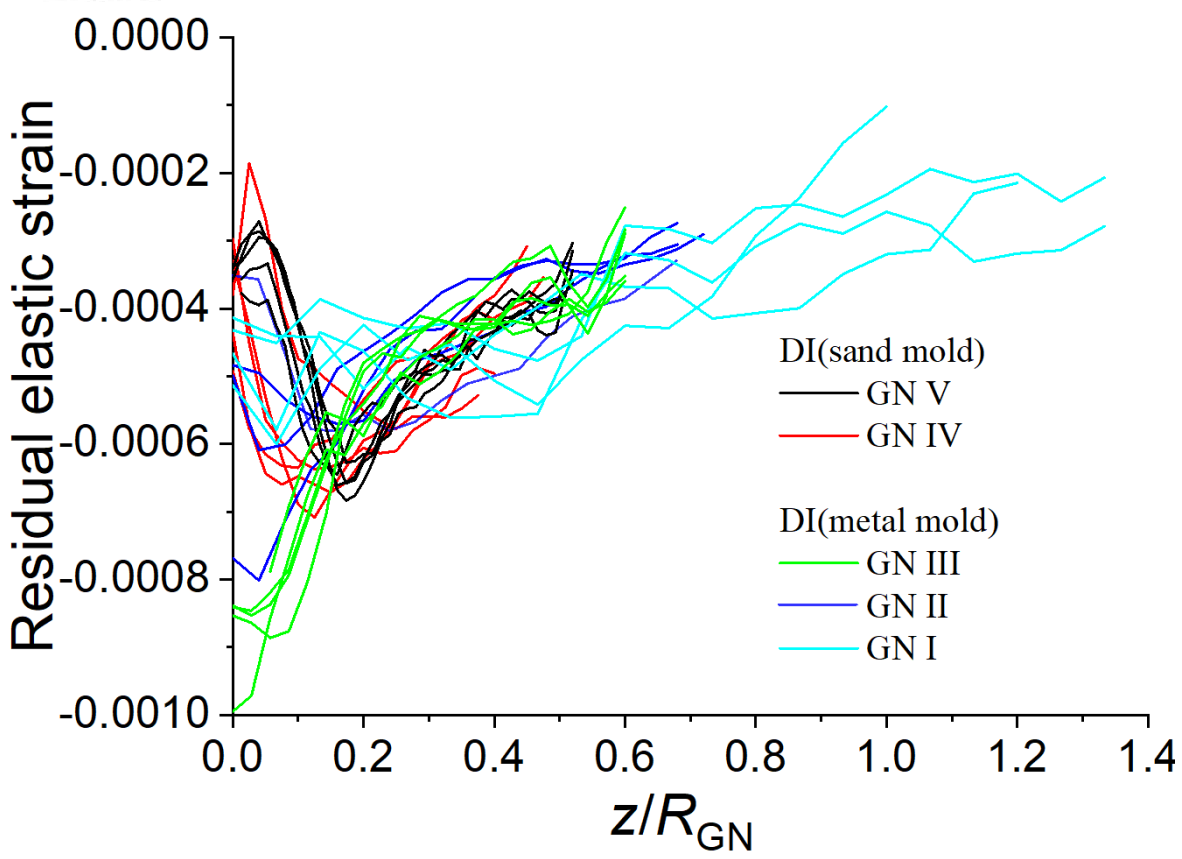

Figure 4. Residual elastic strains as a function of normalized distance from GP/matrix interface (z/R_{GP}) for the different GPs. Reproduced from [43].

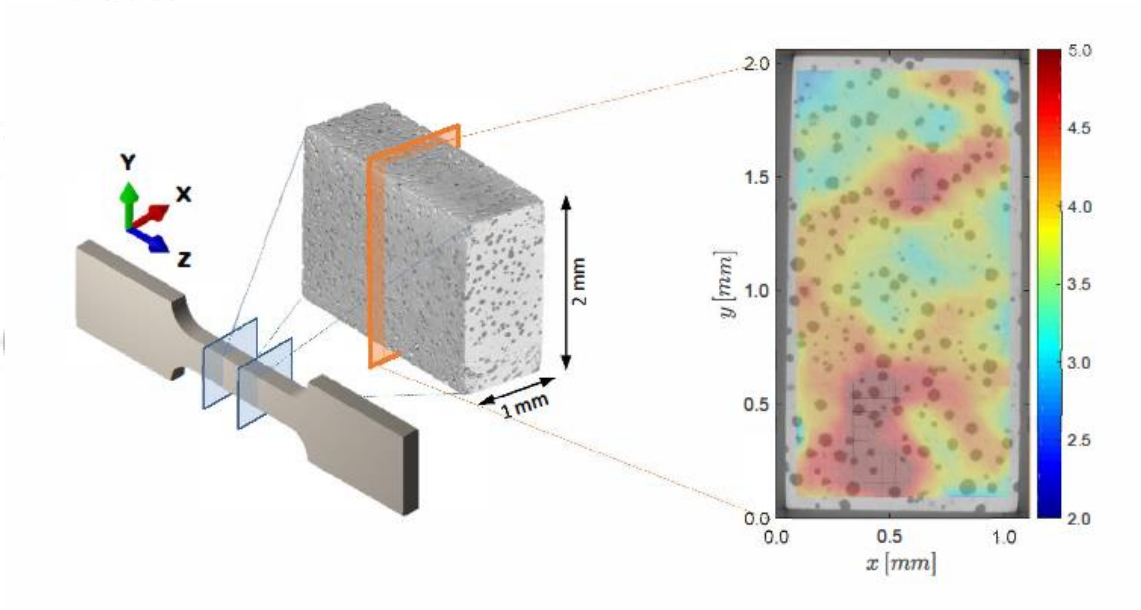

Figure 5. Example of combined use of X-ray CT and DVC. Equivalent strain (in %) over the central cross-section of a tensile DI specimen subjected to 4 % macroscopic deformation, superimposed onto the CT scan of the microstructure. Adapted from [29].

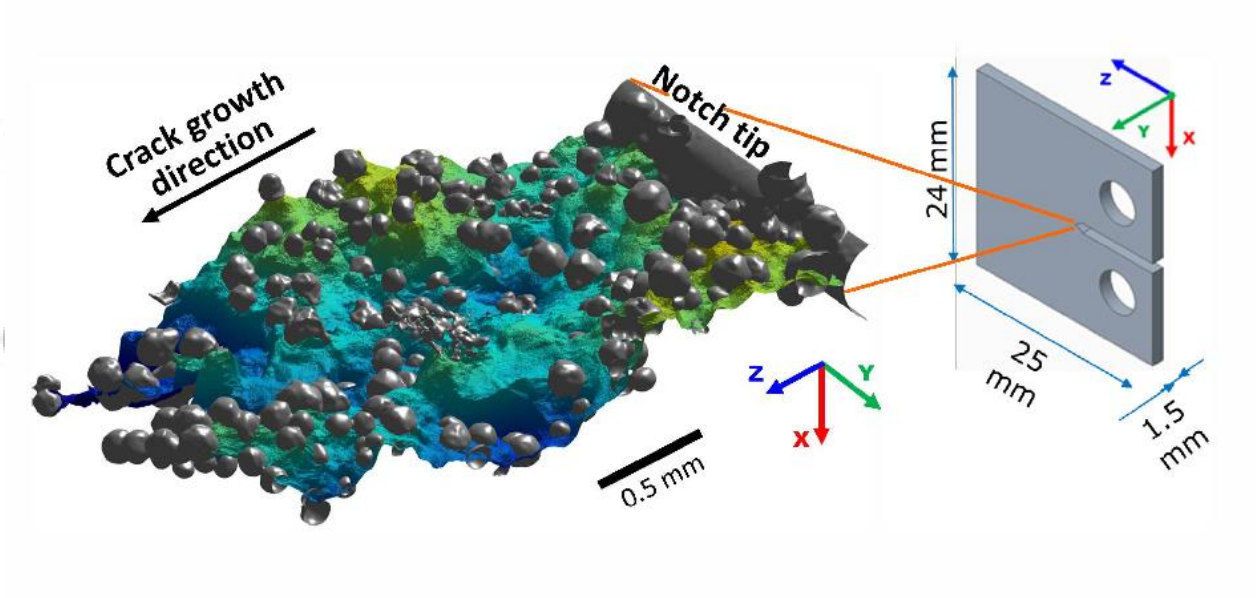

Figure 6. DVC-based reconstruction of a fatigue crack that grows by linking the graphite particles (in gray) in a compact tension specimen. The crack color is proportional to the distance from the ideal crack propagation plane that is perpendicular to the X-axis. Adapted from [71].